

Momentum-GS: Momentum Gaussian Self-Distillation for High-Quality Large Scene Reconstruction

Jixuan Fan^{1,*}, Wanhua Li^{2,*}, Yifei Han¹, Yansong Tang^{1,✉}

¹Tsinghua Shenzhen International Graduate School, Tsinghua University ²Harvard University

fjx23@mails.tsinghua.edu.cn, wanhua@seas.harvard.edu, hyf23@mails.tsinghua.edu.cn

tang.yansong@sz.tsinghua.edu.cn

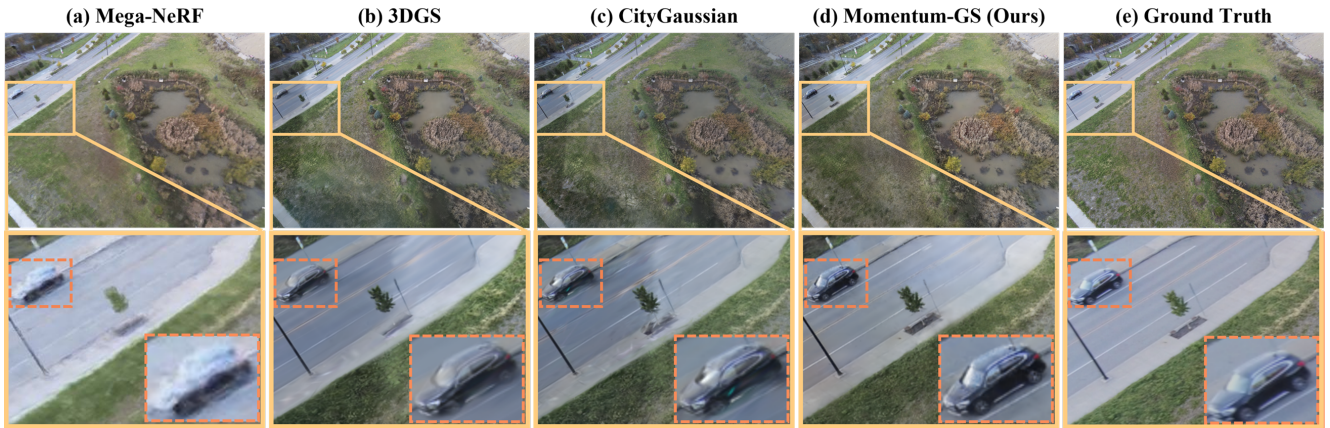


Figure 1. Comparison of reconstruction results on the Rubble [50] dataset. **Momentum-GS** reconstructs finer details, such as the clear structure of the vehicle in the zoomed-in view. Additionally, our method produces smoother transitions across blocks, demonstrating better consistency and avoiding the noticeable lighting discrepancies observed in other Gaussian-based methods.

Abstract

3D Gaussian Splatting has demonstrated notable success in large-scale scene reconstruction, but challenges persist due to high training memory consumption and storage overhead. Hybrid representations that integrate implicit and explicit features offer a way to mitigate these limitations. However, when applied in parallelized block-wise training, two critical issues arise since reconstruction accuracy deteriorates due to reduced data diversity when training each block independently, and parallel training restricts the number of divided blocks to the available number of GPUs. To address these issues, we propose Momentum-GS, a novel approach that leverages momentum-based self-distillation to promote consistency and accuracy across the blocks while decoupling the number of blocks from the physical GPU count. Our method maintains a teacher Gaussian decoder updated with momentum, ensuring a stable reference during training. This teacher provides each block with global guidance in a self-distillation manner, promot-

ing spatial consistency in reconstruction. To further ensure consistency across the blocks, we incorporate block weighting, dynamically adjusting each block’s weight according to its reconstruction accuracy. Extensive experiments on large-scale scenes show that our method consistently outperforms existing techniques, achieving a 12.8% improvement in LPIPS over CityGaussian with much fewer divided blocks and establishing a new state of the art. Project page: https://jixuan-fan.github.io/Momentum-GS_Page/

1. Introduction

Large-scale 3D scene reconstruction is essential for a wide range of applications, including autonomous driving [24, 40, 48, 57], virtual reality [15, 17], environmental monitoring [30, 56], and aerial surveying [5, 6, 46]. The ability to accurately reconstruct large, complex scenes from collections of images is critical for creating realistic, navigable 3D models and supporting high-quality visualization, analysis, and simulation [8, 18, 21, 32].

3D Gaussian Splatting (3D-GS) [19] has recently gained

* Equal contribution. ✉ Corresponding authors.

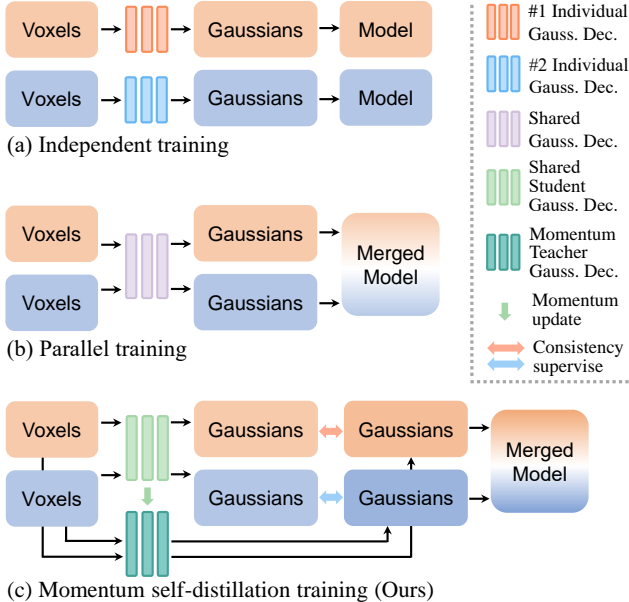


Figure 2. **Comparison of three approaches for using hybrid representations to reconstruct large-scale scenes in a divide-and-conquer manner.** Examples with two blocks: (a) Independent training of each block, resulting in separate models that cannot be merged due to independent Gaussian Decoders, complicating rendering; (b) Parallel training with a shared Gaussian decoder, allowing merged output but limited by GPU availability; (c) Our approach with a Momentum Gaussian Decoder, providing global guidance to each block and improving consistency across blocks.

attention for its high reconstruction quality and fast rendering speed, outperforming NeRF-based methods[2, 4, 36]. Building on this foundation, recent methods [9, 20, 27, 31] have further enhanced its performance on large-scale scenes. To handle large environments more efficiently, these approaches often employ a divide-and-conquer strategy that partitions a large scene into multiple independent blocks, allowing for multi-GPU training across these blocks. This method facilitates scalable training for complex, expansive reconstructions. However, representing millions of Gaussians explicitly creates substantial memory and storage demands [31], limiting the scalability of 3D-GS for extensive scenes. Additionally, due to unavoidable factors in large scene capture, such as lighting variations, auto-exposure adjustments, or inaccuracies in camera poses [23], independently training each block often disregards inter-block relationships, leading to inconsistencies across block boundaries. This issue can result in visible transitions, as seen in Fig. 1 with methods like CityGaussian[31], where abrupt lighting variations are incorrectly rendered. Addressing these concerns has become a core focus in advancing the field of 3D scene reconstruction.

Hybrid representations [26, 33, 43] have emerged as a

promising approach to address memory and storage limitations by combining implicit and explicit features. To manage the complexity of large scenes, these representations integrate dense voxel grids or anchor-based structures with sparse 3D Gaussian fields. These methods typically use MLP as the Gaussian decoder, enabling the generation of neural Gaussians that achieve high reconstruction accuracy while ensuring efficient inference. The decoded Gaussians adapt dynamically to different viewing angles, distances, and scene details. For instance, in Scaffold-GS [33], during inference, the prediction of neural Gaussians is restricted to anchors within the visible frustum, and trivial Gaussians are filtered out based on opacity using a learned selection process. This approach enables rendering speeds comparable to the original 3D-GS. Additionally, neural Gaussians are generated on-the-fly within the view frustum, allowing each anchor to adaptively predict Gaussians for diverse viewing directions and distances in real time. This adaptive mechanism enhances the robustness of novel view synthesis, delivering high-quality renderings across various perspectives while keeping acceptable computational overhead.

However, applying hybrid representations in parallelized reconstruction for large 3D scenes presents two main challenges. First, training each block independently limits data diversity within each block’s Gaussian decoder, reducing reconstruction quality and producing separate models that cannot be merged due to their independent Gaussian decoders, as illustrated in Fig. 2 (a). In contrast, parallel training with a shared Gaussian decoder, as in Fig. 2 (b), allows for merging the trained models but constrains scalability, as the number of blocks is limited by the available GPUs. These limitations underscore the need for an approach that balances inter-block consistency with scalability.

To overcome these limitations, we propose Momentum-GS, a novel approach that combines the benefits of hybrid representations with a strategy tailored to meet the unique demands of large-scale scene reconstruction. Our method decouples the number of blocks from GPU constraints, allowing flexible scaling of reconstruction tasks. This is achieved by periodically sampling k blocks from a set of n blocks and distributing them across k GPUs. To enhance consistency between blocks, we introduce scene momentum self-distillation, where a teacher Gaussian decoder, updated with momentum, provides consistent global guidance to each block, as depicted in Fig. 2 (c). This framework encourages collaborative learning across blocks, ensuring that each block benefits from the broader context of the entire scene. Additionally, we introduce reconstruction-guided block weighting, a dynamic mechanism that adjusts the emphasis on each block based on its reconstruction quality. This adaptive weighting enables the shared decoder to prioritize underperforming blocks, enhancing global consistency and preventing convergence to local minima.

To thoroughly evaluate the effectiveness of the proposed method, we conduct extensive experiments on five challenging large-scale scenes [25, 28, 50], including Building, Rubble, Residence, Sci-Art, and MatrixCity. Our Momentum-GS achieves substantial improvements, demonstrating a 12.8% gain in LPIPS over CityGaussian [31] while utilizing much fewer divided blocks.

In summary, our contributions are:

1. We introduce scene momentum self-distillation to enhance Gaussian decoder performance and decouples the number of divided blocks from the number of GPUs, enabling scalable parallel training.
2. Our approach incorporates reconstruction-guided block weighting, dynamically adjusting block emphasis based on reconstruction quality to ensure focused improvement on weaker blocks, enhancing overall consistency.
3. Our approach, Momentum-GS, achieves better reconstruction quality than state-of-the-art methods, highlighting the strong potential of hybrid representations for large-scale scene reconstruction.

2. Related work

Neural Rendering. Neural Radiance Fields (NeRF)[36] have pioneered a breakthrough in novel view synthesis by representing a 3D scene as a continuous volumetric function, where each point along an emitted ray is sampled to produce color and density values. NeRF optimizes this representation by training a neural network on large sets of posed images, enabling realistic image generation from novel viewpoints. Numerous extensions [2–4, 34, 37, 39, 41, 42, 49, 54] have been developed to improve various aspects of NeRF, including its efficiency and scalability. However, NeRFs require intensive sampling along rays for accurate results, leading to high computational costs and prolonged training and inference times. 3D Gaussian Splatting[19] has emerged as a promising alternative, leveraging Gaussian splats for efficient scene representation. Compared to NeRFs, 3D-GS significantly reduces sampling requirements while maintaining high fidelity, making it more suitable for real-time applications. Another approach, hybrid representation, combines explicit and implicit elements to benefit from the strengths of both[26, 38, 43, 45, 51]. Often constructed on dense, uniform voxel grids, hybrid representations leverage a mix of methods to improve scene reconstruction. For instance, K-Planes [14] uses planar factorization to represent multi-dimensional scenes, supporting efficient memory use and applying priors like temporal smoothness. Plenoxels [13] adopts a sparse 3D grid with spherical harmonics, bypassing neural networks to directly optimize photorealistic view synthesis from images, achieving significant speedups over traditional radiance fields. Scaffold-GS [33] builds on 3D Gaussian Splatting by using anchor points to distribute local

3D Gaussians and predict their attributes dynamically based on viewing direction and distance. These hybrid approaches showcase the advantages of combining explicit and implicit elements for scalable, efficient scene reconstruction.

Large Scene Reconstruction. Large-scale scene reconstruction has a long history, with traditional methods often relying on Structure-from-Motion (SfM) [1, 47] to estimate camera poses and create a sparse point cloud from image collections. Subsequent methods, such as Multi-View Stereo (MVS), expanded on this foundation to produce denser reconstructions, advancing the capability of photogrammetry systems to handle large scenes. With the advent of Neural Radiance Fields (NeRF) [36], a shift toward neural representations for photo-realistic view synthesis has enabled more detailed scene reconstructions. Many NeRF-based approaches[23, 35, 48, 50, 55, 61], use a similar divide-and-conquer approach, representing each block independently to facilitate scalable reconstruction. However, these methods still face challenges in rendering speed and consistency across scene segments. Recently, 3D Gaussian Splatting[19] has emerged as a promising alternative, offering real-time rendering with high visual fidelity. Numerous methods extend 3D-GS to large-scale scenes by enhancing its scalability and efficiency[7, 10–12, 16, 22, 29, 44, 52, 58]. Some methods[9, 20, 27, 31, 59] partition these large scenes into independent blocks for parallel training, allowing for efficient processing and reconstruction. VastGaussian and CityGaussian, by employing a divide-and-conquer approach to reconstruct large-scale scenes, effectively ensure training convergence, though they lack cross-block interaction, which may limit consistency. DOGS introduces a distributed training method that accelerates 3D-GS through scene decomposition and ADMM, while not focusing on optimizing the Gaussian representation for large-scale scenes. These recent 3D-GS-based methods demonstrate the potential of 3D Gaussian representations for scalable, high-quality large scene reconstruction, though challenges remain in achieving seamless transitions and efficient memory usage.

3. Methods

Overview. Hybrid representations have demonstrated success in small, object-centric scenes. However, when applied to parallel training in a divide-and-conquer manner for larger environments, they encounter a fundamental dilemma. In this paper, we leverage hybrid representations for large-scale scene reconstruction, harnessing their high reconstruction capability while effectively decoupling the number of blocks from the physical GPU count. Section 3.1 introduces the essential foundations of 3D-GS. Section 3.2 then explores how Scene Momentum Self-Distillation effectively addresses the challenges of scaling hybrid repre-

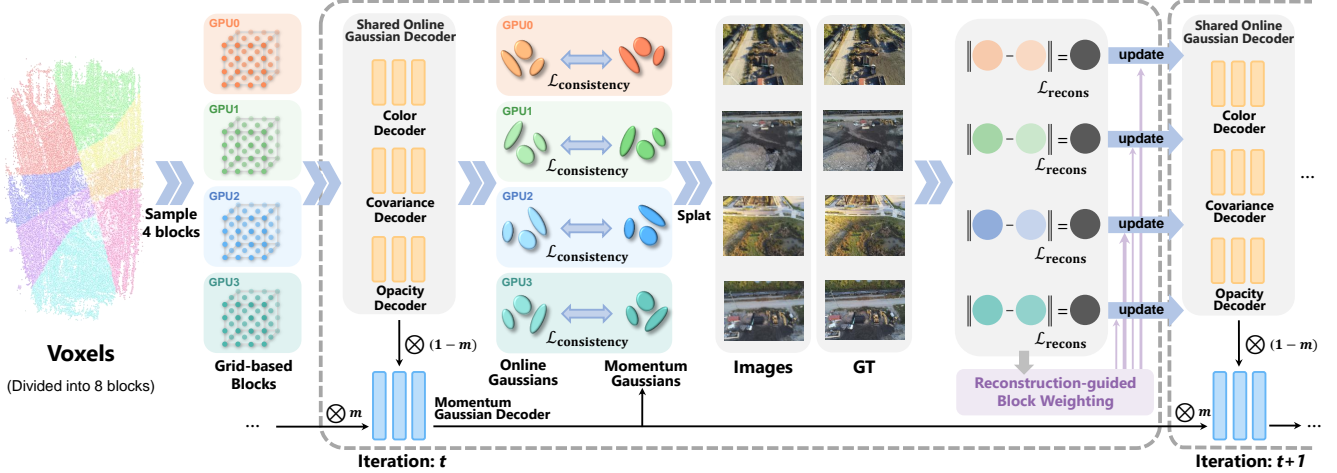


Figure 3. **Overview of the proposed Momentum-GS.** Our method begins by dividing the scene into multiple blocks (left), periodically sampling a subset of blocks (e.g., 4 blocks) and assigning them to available GPUs for parallel processing. The momentum Gaussian decoder provides stable global guidance to each block, ensuring consistency across blocks. To align the online Gaussians with the momentum Gaussian decoder, a consistency loss is applied. During splatting, predicted images are compared with ground truth images, and the resulting reconstruction loss is used to update the shared online Gaussian decoder. Additionally, reconstruction-guided block weighting dynamically adjusts the emphasis on each block, prioritizing underperforming blocks to enhance overall scene consistency.

sentations to large scenes. Lastly, Sec. 3.3 presents the Reconstruction-guided Block Weighting strategy, which enhances global scene consistency by dynamically adjusting each block’s weight based on its reconstruction quality.

3.1. Preliminaries

3D-GS offers an efficient solution for accurate scene reconstruction by leveraging the differentiable properties of Gaussian representations along with tile-based rendering. It models each 3D scene point as an anisotropic Gaussian, allowing for streamlined rendering through projection and blending without the computational overhead of dense ray marching typical in traditional volumetric methods.

Each 3D point is represented as a Gaussian function centered at $\mu \in \mathbb{R}^3$, where x is the spatial position, μ is the center, and Σ defines the Gaussian’s shape and orientation:

$$G(x) = e^{-\frac{1}{2}(x-\mu)^\top \Sigma^{-1}(x-\mu)}. \quad (1)$$

Rendering projects each 3D Gaussian onto the 2D image plane, resulting in a 2D Gaussian $G'(\mathbf{x}')$, where \mathbf{x}' represents a pixel. The projected Gaussian contributes to pixel color via alpha blending:

$$C(\mathbf{x}') = \sum_{i \in N} c_i \sigma_i \prod_{j=1}^{i-1} (1 - \sigma_j), \quad (2)$$

where N is the set of Gaussians affecting \mathbf{x}' , c_i is the color in view-dependent spherical harmonics form, and $\sigma_i = \alpha_i G'_i(\mathbf{x}')$ is the opacity with α_i as a learnable parameter.

The training of Gaussians uses differentiable rendering to refine Gaussian parameters, starting from an initial point cloud. Gaussians are optimized based on image reconstruction error, with operations like cloning, densifying, and pruning to improve coverage and accuracy. For large scenes, the high Gaussian count presents memory and computational challenges, managed by controlling the active Gaussians during rendering.

3.2. Scene-Aware Momentum Self-Distillation

Hybrid representations face a fundamental challenge when applied to parallel training in a divide-and-conquer approach. Specifically, the limitation of GPU availability restricts the number of blocks that can be processed simultaneously, reducing scalability, while the need for data diversity to maintain the Gaussian decoder’s predictive accuracy remains critical. To address these challenges, we propose Scene Momentum Self-Distillation, a method that both decouples the block count from GPU limitations and enhances the Gaussian decoder’s robustness through improved data diversity. Our method ensures that the Gaussian decoder benefits from a broader range of data, enabling more accurate and consistent predictions across large scenes.

In our approach, we train each block simultaneously in parallel, with all blocks sharing a single Gaussian decoder. During each forward pass, each block randomly selects a viewpoint from its assigned data and uses the shared Gaussian decoder to predict the Gaussian parameters accurately. These predicted parameters are then used to render the corresponding image, which is compared to the ground truth

to calculate the reconstruction loss. We optimize the learnable parameters using a loss function that combines the \mathcal{L}_1 loss on rendered pixel colors with an SSIM[53] term $\mathcal{L}_{\text{SSIM}}$, aiming to improve structural similarity:

$$\mathcal{L}_{\text{recons}} = \mathcal{L}_1 + \lambda_{\text{SSIM}}\mathcal{L}_{\text{SSIM}}, \quad (3)$$

where λ_{SSIM} is a weighting factor that balances the contributions of the \mathcal{L}_1 and SSIM terms. The gradients from each block are accumulated into the shared Gaussian decoder, allowing it to learn from the full range of scene information.

To address the GPU-bound limitation on block count, our approach periodically loads a single block onto the GPU, training multiple blocks on each GPU sequentially. After a specified interval, we switch to a different block to continue training. To reduce I/O overhead from switching, we use a relatively large interval, switching blocks every 500 iterations. This method effectively decouples the block count from the number of GPUs, enabling scalable increases in the number of blocks as scene complexity grows.

In order to maintain coherence across staggered training blocks and enhance global consistency, we incorporate a momentum teacher Gaussian decoder D_t alongside a shared student Gaussian decoder D_s . Let B denote the index of each parallel training block, with the parameters of the teacher and student Gaussian decoders represented by θ_t and θ_s , respectively. We employ a self-supervised strategy to stabilize the teacher Gaussian decoder D_t via momentum updates, mitigating inconsistencies introduced by staggered training. The teacher decoder thus serves as a stable global reference, guiding the student decoder through a consistency loss applied between the two.

More formally, the parameters θ_t of the teacher Gaussian decoder are updated using a momentum-based formula that ensures temporal stability:

$$\theta_t \leftarrow m \cdot \theta_t + (1 - m) \cdot \theta_s, \quad (4)$$

where m is the momentum coefficient, set to 0.9 to balance stability and update speed. If m is too close to 1, the decoder updates too slowly, hindering reconstruction efficiency, while a smaller m may lead to instability due to excessive fluctuations in the teacher decoder. This momentum-based update ensures that the teacher Gaussian decoder evolves smoothly, providing stable and consistent guidance to the student decoder across all blocks. For each block, Gaussian parameters are predicted by both the teacher and student decoders, with a consistency loss applied to align the student decoder with the global guidance from the teacher. This approach leverages increased data diversity while decoupling the number of blocks from the GPU count, allowing scalability to arbitrarily large scenes.

The consistency loss is computed as the mean squared error between the predictions of the teacher and student Gaus-

sian decoders for each block B :

$$\mathcal{L}_{\text{consistency}} = \|D_m(f_b, v_b; \theta_t) - D_o(f_b, v_b; \theta_s)\|_2, \quad (5)$$

where f_b represents the anchor feature and v_b the relative viewing direction for each sample within block B . This loss encourages the student decoder D_o to progressively align with the stable global guidance provided by the teacher decoder D_m , promoting spatial consistency across different blocks throughout the reconstruction process.

Thus, the total loss function is defined as:

$$\mathcal{L} = \mathcal{L}_1 + \lambda_{\text{SSIM}}\mathcal{L}_{\text{SSIM}} + \lambda_{\text{consistency}}\mathcal{L}_{\text{consistency}}, \quad (6)$$

where $\lambda_{\text{consistency}}$ is a weighting factor that balances the impact of the consistency loss relative to the reconstruction loss. This combined loss ensures that the model not only reconstructs the scene accurately but also maintains global spatial coherence across blocks.

3.3. Reconstruction-guided Block Weighting

In order to balance training progress across blocks and mitigate issues arising from uneven initial scene partitioning, we introduce Reconstruction-guided Block Weighting. This method dynamically adjusts weights based on each block’s reconstruction quality, enhancing consistency by giving priority to blocks with lower reconstruction accuracy.

To monitor and adjust the reconstruction performance of each block, we maintain a table that tracks key reconstruction metrics, specifically PSNR (Peak Signal-to-Noise Ratio) and SSIM (Structural Similarity Index). These metrics provide quantitative measures of reconstruction quality, with higher values indicating better visual fidelity. To ensure that these metrics reflect stable performance across training iterations, we update them using a momentum-based approach, which smooths fluctuations and provides a more reliable indication of each block’s progress.

Using these momentum-smoothed metrics, we identify the block with the highest reconstruction performance, labeling its PSNR and SSIM values as PSNR_{max} and SSIM_{max} , respectively. These reference values serve as benchmarks for evaluating the relative accuracy of each block. For every block in the scene, we calculate deviations δ_p and δ_s to quantify how closely its reconstruction aligns with the highest-performing block. Specifically, the PSNR deviation δ_p is obtained by subtracting the current block’s PSNR from PSNR_{max} . δ_s is derived similarly.

With these deviations calculated, we assign each block a weight w_i that reflects its relative reconstruction performance. The weight w_i is constructed to resemble a Gaussian distribution, placing greater emphasis on blocks with larger deviations from the best-performing block. By prioritizing blocks with lower reconstruction accuracy, this approach directs the model’s attention to underperforming blocks, helping to improve overall consistency across

the scene. Additionally, w_i is capped within a range slightly above one, which prevents excessively high adjustments, ensuring stable training dynamics and avoiding over-penalization of blocks with moderate deviations.

$$w_i = 2 - \exp\left(\frac{\delta_p^2 + \lambda \cdot \delta_s^2}{-2\sigma^2}\right), \quad (7)$$

This design guiding the Gaussian decoder to focus on the global scene rather than converging on blocks with locally high-quality reconstructions. Consequently improves consistency across all blocks, ultimately enhancing the overall scene reconstruction quality.

4. Experiments

4.1. Experimental Setup

Dataset and Metrics. We conducted experiments on five large-scale scenes across three datasets: Building and Rubble from the Mill19[50] dataset, Residence and Sci-Art from the UrbanScene3D[28] dataset, and Aerial from a small city region within the MatrixCity[25] dataset. Each of these datasets includes thousands of high-resolution images. We used the same scene partitioning as Mega-NeRF[50] and downsampled all images by 4 times, following previous methods[27, 31, 50] for fair comparison. We evaluated reconstruction accuracy using PSNR, SSIM[53], and LPIPS[60] metrics, and additionally reported the storage size (GB) to assess model compactness. Since VastGaussian[27] and DOGS[9] are not open-sourced yet, we were unable to include them in the storage size comparison. Please refer to the supplementary material for additional comparisons, including VRAM usage, storage size, and the number of divided blocks.

Compared methods. We compare our method with six methods, categorized into NeRF-based methods, including Mega-NeRF[50] and Switch-NeRF[35], and gaussian-based methods, including 3D-GS[19], VastGaussian[27], CityGaussian[31], and DOGS[9]. Notably, DOGS’s settings differ slightly from those of the other methods: DOGS downsamples all images by a factor of 6+ and trains for 80,000 iterations, as opposed to the 4 times downsampling and 60,000 training iterations in prior works, which may introduce some performance advantages.

Implementation. Following previous methods[27, 31, 35, 50], we downsample all images by a factor of 4 and train for a total of 60,000 iterations. Anchor points are adjusted from iteration 300 to 30,000 with an interval of 25 iterations. To ensure fair comparisons, we adopt the same scene partitioning strategy as CityGaussian but use notably fewer blocks. Specifically, we divide all scenes into 8 blocks, whereas CityGaussian partitions Building, Rubble, Residence, Sci-Art, and MatrixCity into 20, 9, 20, 9, and 36

blocks, respectively. VastGaussian applies color correction to the rendered images before evaluating metrics, resulting in evidently higher results. To ensure comparability across methods, we report the results of VastGaussian based on a reproduced version[9] without the use of color correction and decoupled appearance encoding.

4.2. Results Analysis

Quantitative Results. In Tab. 1, we report the PSNR, SSIM, and LPIPS metrics across four large-scale scenes. Our Momentum-GS achieves the best performance in SSIM and LPIPS across all scenes, significantly outperforming other methods in terms of perceptual quality. These results suggest that Momentum-GS effectively balances fine detail preservation with high rendering quality. Notably, NeRF-based methods achieve higher PSNR on the Sci-Art dataset. We observe that the Sci-Art dataset suffers from noticeable blur, likely due to out-of-focus capture conditions. NeRF-based methods tend to produce smoother, often slightly blurred reconstructions, which may align more closely with the inherent characteristics of the Sci-Art data, resulting in artificially elevated PSNR scores. However, when considering SSIM and LPIPS, Gaussian-based methods, including our Momentum-GS, outperform NeRF-based approaches, suggesting a superior ability to preserve structural and perceptual details across different scenes.

Visualization Results. In Fig. 4, we provide visual comparisons of reconstruction results across different scenes. Compared to other methods, our Momentum-GS demonstrates superior detail preservation and produces sharper, more realistic images. While other methods often suffer from noticeable blurring or loss of structure in complex areas, our approach achieves clean and well-defined renderings across all scenes. These results highlight the effectiveness of Momentum-GS in capturing fine-grained details and maintaining visual clarity.

4.3. Ablation Studies

Parallel training vs. independent training. In Tab. 4, we demonstrate that parallel training achieves better reconstruction accuracy compared to independent training when the scene is divided into the same number of blocks, due to the increased data diversity accessible to each block’s Gaussian decoder. However, direct parallel training is limited by the constraint that the number of blocks is tied to the number of physical GPUs. As a result, independent training can achieve further accuracy improvements by increasing the number of blocks, whereas simple parallel training cannot. Specifically, we show that dividing the scene into 8 blocks yields better results than 4 blocks in independent training. To increase data diversity in training the Gaussian decoder while decoupling the block count from the GPU count, we introduce scene momentum self-distillation,

| Scene | Building | | | Rubble | | | Residence | | | Sci-Art | | |
|--------------------------------|-----------------|-----------------|--------------------|-----------------|-----------------|--------------------|-----------------|-----------------|--------------------|-----------------|-----------------|--------------------|
| Metrics | PSNR \uparrow | SSIM \uparrow | LPIPS \downarrow | PSNR \uparrow | SSIM \uparrow | LPIPS \downarrow | PSNR \uparrow | SSIM \uparrow | LPIPS \downarrow | PSNR \uparrow | SSIM \uparrow | LPIPS \downarrow |
| Mega-NeRF [50] | 20.93 | 0.547 | 0.504 | 24.06 | 0.553 | 0.516 | 22.08 | 0.628 | 0.489 | <u>25.60</u> | 0.770 | 0.390 |
| Switch-NeRF [35] | 21.54 | 0.579 | 0.474 | 24.31 | 0.562 | 0.496 | 22.57 | 0.654 | 0.457 | 26.52 | 0.795 | 0.360 |
| 3D-GS [19] | 20.46 | 0.720 | 0.305 | 25.47 | 0.777 | 0.277 | 21.44 | 0.791 | 0.236 | 21.05 | 0.830 | 0.242 |
| VastGaussian [†] [27] | 21.80 | 0.728 | 0.225 | 25.20 | 0.742 | 0.264 | 21.01 | 0.699 | 0.261 | 22.64 | 0.761 | 0.261 |
| CityGaussian [31] | 21.55 | <u>0.778</u> | 0.246 | 25.77 | <u>0.813</u> | <u>0.228</u> | 22.00 | <u>0.813</u> | <u>0.211</u> | 21.39 | <u>0.837</u> | 0.230 |
| DOGS* [9] | <u>22.73</u> | 0.759 | <u>0.204</u> | <u>25.78</u> | 0.765 | 0.257 | 21.94 | 0.740 | 0.244 | 24.42 | 0.804 | <u>0.219</u> |
| Momentum-GS (Ours) | 23.23 | 0.815 | 0.194 | 25.93 | 0.827 | 0.201 | <u>22.21</u> | 0.818 | 0.197 | 23.02 | 0.856 | 0.205 |

Table 1. Quantitative comparison of our Momentum-GS against prior methods across four large-scale scenes. We present metrics for PSNR \uparrow , SSIM \uparrow , and LPIPS \downarrow on test views. The **best** and second best scores are highlighted. \dagger denotes without applying the decoupled appearance encoding, * indicates that the experimental setting has minor differences from other methods.

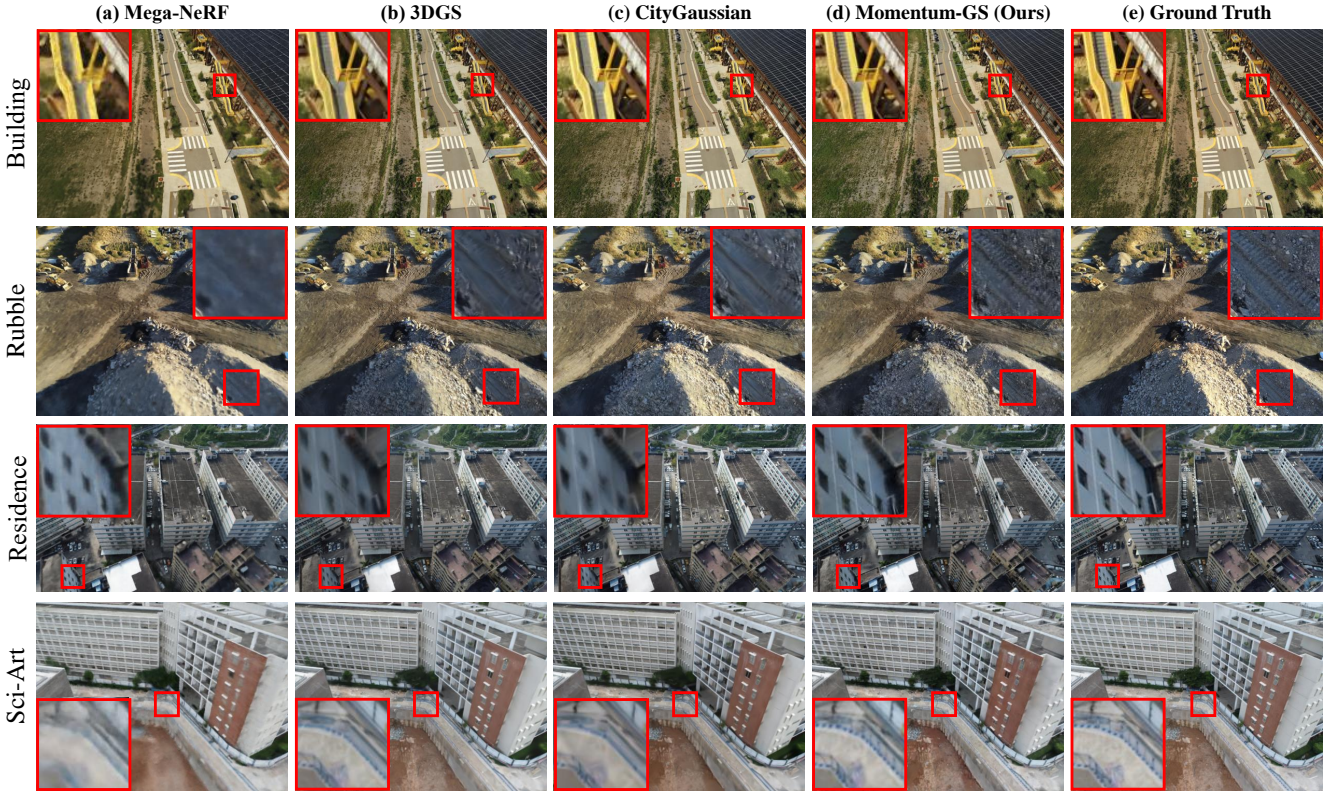


Figure 4. Qualitative comparisons of our Momentum-GS and prior methods across four large-scale scenes. Red insets highlight patches that reveal notable visual differences between these methods. Our method (d) demonstrates better fidelity in capturing fine details, maintaining structural consistency, and accurately representing textures. This results in visual reconstructions that are closer to the ground truth (e) compared to Mega-NeRF (a), 3D-GS (b), and CityGaussian (c), which exhibit artifacts, blurring, or inconsistencies in these areas.

which significantly improves accuracy compared to training 8 blocks independently. Additionally, reconstruction quality can be further enhanced by incorporating reconstruction-guided block weighting (denoted as "Full" in Tab. 4).

Block weighting. In Tab. 3, we evaluate different methods for measuring the reconstruction quality of each block. Our results show that incorporating both PSNR and SSIM yields better accuracy compared to relying solely on either metric.

Scalability. We evaluated our method on various numbers of divided blocks, keeping the number of GPUs constant as four. The results, shown in Table 5, demonstrate a consistent improvement in reconstruction accuracy as the number of blocks increases. This indicates that our method can effectively scale to train on any desired number of blocks, even with limited GPU resources. Our approach outperforms CityGaussian, achieving superior accu-

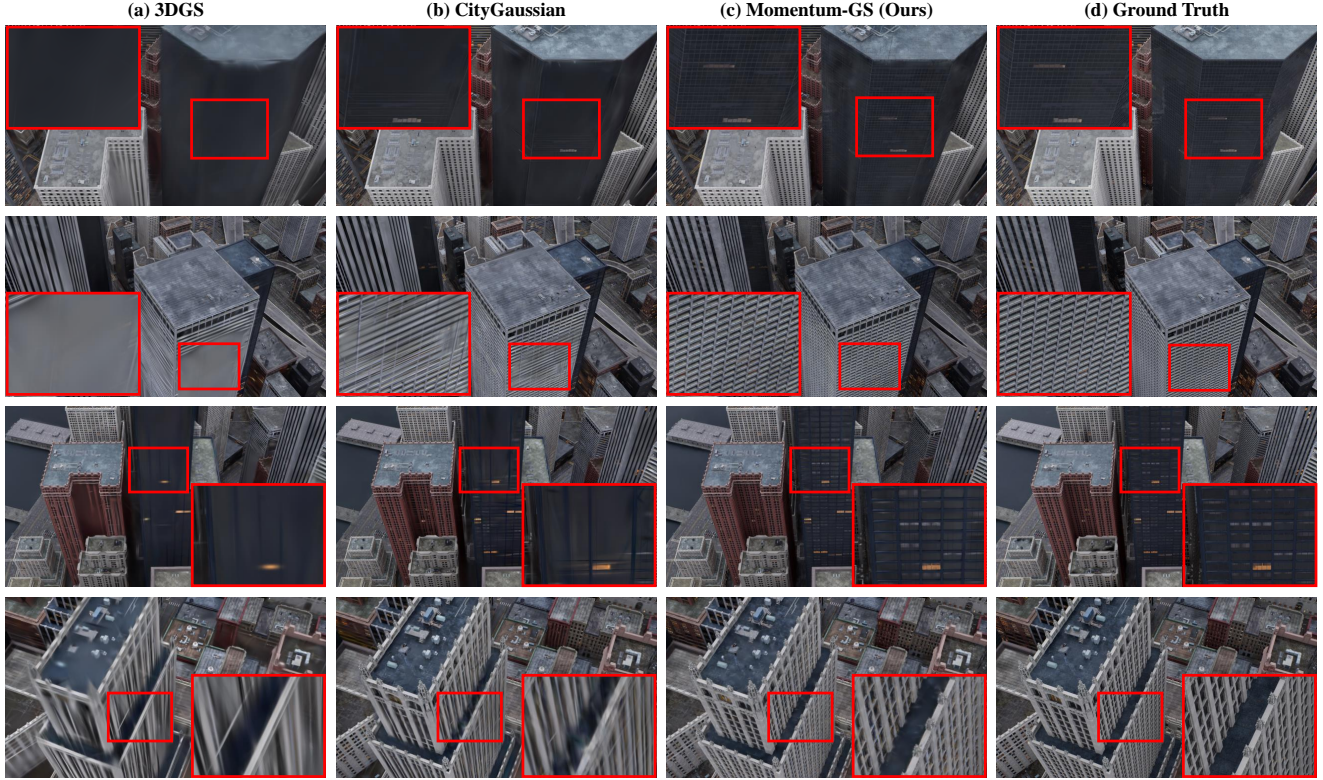


Figure 5. Qualitative comparisons of our Momentum-GS and other methods on a large-scale urban scene MatrixCity. Our method (c) demonstrates greater detail preservation in challenging regions such as building facades and edges, closely matching the ground truth (d). In contrast, 3D-GS (a) and CityGaussian (b) exhibit obvious artifacts, blurring, or loss of structural detail in these areas.

| Method | PSNR | SSIM | LPIPS | #Block | Mem (GB) |
|---------------------------|--------------|--------------|--------------|--------|-------------|
| 3D-GS [19] | 23.67 | 0.735 | 0.384 | 1 | 2.40 |
| CityGaussian [31] | 27.46 | 0.865 | 0.204 | 36 | 5.40 |
| Momentum-GS (Ours) | 28.01 | 0.880 | 0.179 | 8 | 2.08 |

Table 2. Quantitative comparison of our Momentum-GS against prior methods on the MatrixCity dataset. We report PSNR \uparrow , SSIM \uparrow , and LPIPS \downarrow on test views, with the **best** results highlighted. The number of divided blocks and the storage size are additionally reported for each method.

| Models | PSNR | SSIM | LPIPS |
|---------------------------|--------------|--------------|--------------|
| w/ PSNR | 23.03 | 0.812 | 0.196 |
| w/ SSIM | 23.00 | 0.807 | 0.203 |
| Full (PSNR + SSIM) | 23.23 | 0.815 | 0.194 |

Table 3. Ablation study on different strategy of measuring the reconstruction quality in block weighting.

racy with fewer blocks, highlighting its scalability and effectiveness in large-scale scene reconstruction.

| Training strategy | #Block | PSNR | SSIM | LPIPS |
|-------------------------------|----------|--------------|--------------|--------------|
| baseline | 1 | 21.52 | 0.741 | 0.280 |
| w/ Parallel training | 4 | 22.62 | 0.790 | 0.227 |
| w/ Independent training | 4 | 22.50 | 0.787 | 0.227 |
| w/ Independent training | 8 | 22.68 | 0.799 | 0.212 |
| w/ momentum self-distillation | 8 | 23.05 | 0.807 | 0.205 |
| Full | 8 | 23.23 | 0.815 | 0.194 |

Table 4. Ablation study on different training strategies.

| Method | #Block | PSNR | SSIM | LPIPS |
|--------------------|--------|-------|-------|-------|
| CityGaussian | 32 | 27.46 | 0.865 | 0.204 |
| Momentum-GS (Ours) | 4 | 27.87 | 0.869 | 0.203 |
| Momentum-GS (Ours) | 8 | 28.01 | 0.880 | 0.179 |
| Momentum-GS (Ours) | 16 | 28.02 | 0.883 | 0.170 |

Table 5. Ablation study on the number of blocks used in our Momentum-GS compared to CityGaussian.

5. Conclusion

In this paper, we have introduced Momentum-GS, a novel momentum-based self-distillation framework that notably enhances 3D Gaussian Splatting for large-scale scene reconstruction. The core of Momentum-GS is a momentum-

updated teacher Gaussian decoder, which serves as a stable global reference to guide parallel training blocks, effectively promoting spatial consistency and coherence across the reconstructed scene. We further introduce a reconstruction-guided block weighting mechanism, which dynamically adjusts the emphasis on each block based on reconstruction quality, further improving overall consistency. Our approach leverages hybrid representations, integrating both implicit and explicit features, to enable flexible scaling that decouples the number of blocks from GPU constraints. Experimental results demonstrate the strong capability of hybrid representations and momentum-based self-distillation for robust, large-scale 3D scene reconstruction.

References

- [1] Sameer Agarwal, Yasutaka Furukawa, Noah Snavely, Ian Simon, Brian Curless, Steven M Seitz, and Richard Szeliski. Building rome in a day. *Communications of the ACM*, 54(10):105–112, 2011. 3
- [2] Jonathan T. Barron, Ben Mildenhall, Matthew Tancik, Peter Hedman, Ricardo Martin-Brualla, and Pratul P. Srinivasan. Mip-nerf: A multiscale representation for anti-aliasing neural radiance fields. In *ICCV*, pages 5855–5864, 2021. 2, 3
- [3] Jonathan T Barron, Ben Mildenhall, Dor Verbin, Pratul P Srinivasan, and Peter Hedman. Mip-nerf 360: Unbounded anti-aliased neural radiance fields. In *CVPR*, pages 5470–5479, 2022.
- [4] Jonathan T Barron, Ben Mildenhall, Dor Verbin, Pratul P Srinivasan, and Peter Hedman. Zip-nerf: Anti-aliased grid-based neural radiance fields. In *ICCV*, pages 19697–19705, 2023. 2, 3
- [5] Ilker Bozcan and Erdal Kayacan. Au-air: A multi-modal unmanned aerial vehicle dataset for low altitude traffic surveillance. In *2020 IEEE International Conference on Robotics and Automation (ICRA)*, pages 8504–8510. IEEE, 2020. 1
- [6] Guikun Chen and Wenguan Wang. A survey on 3d gaussian splatting. *arXiv preprint arXiv:2401.03890*, 2024. 1
- [7] Junyi Chen, Weicai Ye, Yifan Wang, Danpeng Chen, Di Huang, Wanli Ouyang, Guofeng Zhang, Yu Qiao, and Tong He. Gigags: Scaling up planar-based 3d gaussians for large scene surface reconstruction. *arXiv preprint arXiv:2409.06685*, 2024. 3
- [8] Timothy Chen, Ola Shorinwa, Joseph Bruno, Javier Yu, Weijia Zeng, Keiko Nagami, Philip Dames, and Mac Schwager. Splat-nav: Safe real-time robot navigation in gaussian splatting maps. *arXiv preprint arXiv:2403.02751*, 2024. 1
- [9] Yu Chen and Gim Hee Lee. Dogs: Distributed-oriented gaussian splatting for large-scale 3d reconstruction via gaussian consensus. In *NeurIPS*, 2024. 2, 3, 6, 7, 1
- [10] Jiadi Cui, Junming Cao, Yuhui Zhong, Liao Wang, Fuqiang Zhao, Penghao Wang, Yifan Chen, Zhipeng He, Lan Xu, Yujiao Shi, et al. Letsgo: Large-scale garage modeling and rendering via lidar-assisted gaussian primitives. *arXiv preprint arXiv:2404.09748*, 2024. 3
- [11] Xiao Cui, Weicai Ye, Yifan Wang, Guofeng Zhang, Wengang Zhou, Tong He, and Houqiang Li. Streetsurfs: Scalable urban street surface reconstruction with planar-based gaussian splatting. *arXiv preprint arXiv:2410.04354*, 2024.
- [12] Guofeng Feng, Siyan Chen, Rong Fu, Zimu Liao, Yi Wang, Tao Liu, Zhilin Pei, Hengjie Li, Xingcheng Zhang, and Bo Dai. Flashgs: Efficient 3d gaussian splatting for large-scale and high-resolution rendering. *arXiv preprint arXiv:2408.07967*, 2024. 3
- [13] Sara Fridovich-Keil, Alex Yu, Matthew Tancik, Qinhong Chen, Benjamin Recht, and Angjoo Kanazawa. Plenoxels: Radiance fields without neural networks. In *CVPR*, pages 5501–5510, 2022. 3
- [14] Sara Fridovich-Keil, Giacomo Meanti, Frederik Rahbæk Warburg, Benjamin Recht, and Angjoo Kanazawa. K-planes: Explicit radiance fields in space, time, and appearance. In *CVPR*, pages 12479–12488, 2023. 3
- [15] Jiaming Gu, Minchao Jiang, Hongsheng Li, Xiaoyuan Lu, Guangming Zhu, Syed Afaq Ali Shah, Liang Zhang, and Mohammed Bannamoun. Ue4-nerf: Neural radiance field for real-time rendering of large-scale scene. *NeurIPS*, 36, 2024. 1
- [16] Changjian Jiang, Ruilan Gao, Kele Shao, Yue Wang, Rong Xiong, and Yu Zhang. Li-gs: Gaussian splatting with lidar incorporated for accurate large-scale reconstruction. *arXiv preprint arXiv:2409.12899*, 2024. 3
- [17] Ying Jiang, Chang Yu, Tianyi Xie, Xuan Li, Yutao Feng, Huamin Wang, Minchen Li, Henry Lau, Feng Gao, Yin Yang, et al. Vr-gs: A physical dynamics-aware interactive gaussian splatting system in virtual reality. In *ACM SIGGRAPH 2024 Conference Papers*, pages 1–1, 2024. 1
- [18] Rui Jin, Yuman Gao, Yingjian Wang, Haojian Lu, and Fei Gao. Gs-planner: A gaussian-splatting-based planning framework for active high-fidelity reconstruction. *arXiv preprint arXiv:2405.10142*, 2024. 1
- [19] Bernhard Kerbl, Georgios Kopanas, Thomas Leimkühler, and George Drettakis. 3d gaussian splatting for real-time radiance field rendering. *TOG*, 42(4), 2023. 1, 3, 6, 7, 8
- [20] Bernhard Kerbl, Andreas Meuleman, Georgios Kopanas, Michael Wimmer, Alexandre Lanvin, and George Drettakis. A hierarchical 3d gaussian representation for real-time rendering of very large datasets. *TOG*, 43(4):1–15, 2024. 2, 3
- [21] Xiaohan Lei, Min Wang, Wengang Zhou, and Houqiang Li. Gaussnav: Gaussian splatting for visual navigation. *arXiv preprint arXiv:2403.11625*, 2024. 1
- [22] Bingling Li, Shengyi Chen, Luchao Wang, Kaimin Liao, Si-jie Yan, and Yuanjun Xiong. Retinags: Scalable training for dense scene rendering with billion-scale 3d gaussians. *arXiv preprint arXiv:2406.11836*, 2024. 3
- [23] Ruilong Li, Sanja Fidler, Angjoo Kanazawa, and Francis Williams. NeRF-XL: Scaling nerfs with multiple GPUs. In *ECCV*, 2024. 2, 3
- [24] Wei Li, CW Pan, Rong Zhang, JP Ren, YX Ma, Jin Fang, FL Yan, QC Geng, XY Huang, HJ Gong, et al. Aads: Augmented autonomous driving simulation using data-driven algorithms. *Science robotics*, 4(28):eaaw0863, 2019. 1
- [25] Yixuan Li, Lihan Jiang, Linning Xu, Yuanbo Xiangli, Zhenzhi Wang, Dahua Lin, and Bo Dai. Matrixcity: A large-scale

- city dataset for city-scale neural rendering and beyond. In *ICCV*, pages 3205–3215, 2023. 3, 6, 1
- [26] Zhuopeng Li, Yilin Zhang, Chenming Wu, Jianke Zhu, and Liangjun Zhang. Ho-gaussian: Hybrid optimization of 3d gaussian splatting for urban scenes. *arXiv preprint arXiv:2403.20032*, 2024. 2, 3
- [27] Jiaqi Lin, Zhihao Li, Xiao Tang, Jianzhuang Liu, Shiyong Liu, Jiayue Liu, Yangdi Lu, Xiaofei Wu, Songcen Xu, Youliang Yan, and Wenming Yang. Vastgaussian: Vast 3d gaussians for large scene reconstruction. In *CVPR*, 2024. 2, 3, 6, 7, 1
- [28] Liqiang Lin, Yilin Liu, Yue Hu, Xingguang Yan, Ke Xie, and Hui Huang. Capturing, reconstructing, and simulating: the urbanscene3d dataset. In *ECCV*, pages 93–109, 2022. 3, 6, 1
- [29] Jinpeng Liu, Jiale Xu, Weihao Cheng, Yiming Gao, Xintao Wang, Ying Shan, and Yansong Tang. Novelgs: Consistent novel-view denoising via large gaussian reconstruction model. *arXiv preprint arXiv:2411.16779*, 2024. 3
- [30] Shuhong Liu, Xiang Chen, Hongming Chen, Quanfeng Xu, and Mingrui Li. Deraings: Gaussian splatting for enhanced scene reconstruction in rainy. *arXiv preprint arXiv:2408.11540*, 2024. 1
- [31] Yang Liu, He Guan, Chuanchen Luo, Lue Fan, Naiyan Wang, Junran Peng, and Zhaoxiang Zhang. Citygaussian: Real-time high-quality large-scale scene rendering with gaussians. In *ECCV*, 2024. 2, 3, 6, 7, 8, 1
- [32] Guanxing Lu, Shiyi Zhang, Ziwei Wang, Changliu Liu, Jiwen Lu, and Yansong Tang. Manigaussian: Dynamic gaussian splatting for multi-task robotic manipulation. In *ECCV*, pages 349–366, 2025. 1
- [33] Tao Lu, Mulin Yu, Linning Xu, Yuanbo Xiangli, Limin Wang, Dahua Lin, and Bo Dai. Scaffold-gs: Structured 3d gaussians for view-adaptive rendering. In *CVPR*, pages 20654–20664, 2024. 2, 3
- [34] Ricardo Martin-Brualla, Noha Radwan, Mehdi SM Sajjadi, Jonathan T Barron, Alexey Dosovitskiy, and Daniel Duckworth. Nerf in the wild: Neural radiance fields for unconstrained photo collections. In *CVPR*, pages 7210–7219, 2021. 3
- [35] Zhenxing Mi and Dan Xu. Switch-nerf: Learning scene decomposition with mixture of experts for large-scale neural radiance fields. In *ICLR*, 2023. 3, 6, 7, 1
- [36] Ben Mildenhall, Pratul P Srinivasan, Matthew Tancik, Jonathan T Barron, Ravi Ramamoorthi, and Ren Ng. Nerf: Representing scenes as neural radiance fields for view synthesis. *Communications of the ACM*, 65(1):99–106, 2021. 2, 3
- [37] Ben Mildenhall, Peter Hedman, Ricardo Martin-Brualla, Pratul P Srinivasan, and Jonathan T Barron. Nerf in the dark: High dynamic range view synthesis from noisy raw images. In *CVPR*, pages 16190–16199, 2022. 3
- [38] Thomas Müller, Alex Evans, Christoph Schied, and Alexander Keller. Instant neural graphics primitives with a multiresolution hash encoding. *TOG*, 41(4):1–15, 2022. 3
- [39] Michael Niemeyer, Jonathan T Barron, Ben Mildenhall, Mehdi SM Sajjadi, Andreas Geiger, and Noha Radwan. Regularizing neural radiance fields for view synthesis from sparse inputs. In *CVPR*, pages 5480–5490, 2022. 3
- [40] Julian Ost, Fahim Mannan, Nils Thuerey, Julian Knodt, and Felix Heide. Neural scene graphs for dynamic scenes. In *CVPR*, pages 2856–2865, 2021. 1
- [41] Albert Pumarola, Enric Corona, Gerard Pons-Moll, and Francesc Moreno-Noguer. D-nerf: Neural radiance fields for dynamic scenes. In *CVPR*, pages 10318–10327, 2021. 3
- [42] Christian Reiser, Rick Szeliski, Dor Verbin, Pratul Srinivasan, Ben Mildenhall, Andreas Geiger, Jon Barron, and Peter Hedman. Merf: Memory-efficient radiance fields for real-time view synthesis in unbounded scenes. *TOG*, 42(4):1–12, 2023. 3
- [43] Kerui Ren, Lihan Jiang, Tao Lu, Mulin Yu, Linning Xu, Zhangkai Ni, and Bo Dai. Octree-gs: Towards consistent real-time rendering with lod-structured 3d gaussians. *arXiv preprint arXiv:2403.17898*, 2024. 2, 3
- [44] Xuanchi Ren, Yifan Lu, Hanxue Liang, Jay Zhangjie Wu, Huan Ling, Mike Chen, Francis Fidler, Sanja and Williams, and Jiahui Huang. Scube: Instant large-scale scene reconstruction using voxplats. In *NeurIPS*, 2024. 3
- [45] Jiansong Sha, Haoyu Zhang, Yuchen Pan, Guang Kou, and Xiaodong Yi. Nerf-is: Explicit neural radiance fields in semantic space. In *Proceedings of the 5th ACM International Conference on Multimedia in Asia*, pages 1–7, 2023. 3
- [46] Surendra Pal Singh, Kamal Jain, and V Ravibabu Mandla. 3d scene reconstruction from video camera for virtual 3d city modeling. *American Journal of Engineering Research*, 3(1): 140–148, 2014. 1
- [47] Noah Snavely, Steven M. Seitz, and Richard Szeliski. *Photo Tourism: Exploring Photo Collections in 3D*. Association for Computing Machinery, 2023. 3
- [48] Matthew Tancik, Vincent Casser, Xinchen Yan, Sabeek Pradhan, Ben Mildenhall, Pratul P Srinivasan, Jonathan T Barron, and Henrik Kretzschmar. Block-nerf: Scalable large scene neural view synthesis. In *CVPR*, pages 8248–8258, 2022. 1, 3
- [49] Matthew Tancik, Ethan Weber, Evonne Ng, Ruilong Li, Brent Yi, Terrance Wang, Alexander Kristoffersen, Jake Austin, Kamyar Salahi, Abhik Ahuja, et al. Nerfstudio: A modular framework for neural radiance field development. In *ACM SIGGRAPH 2023 Conference Proceedings*, pages 1–12, 2023. 3
- [50] Haithem Turki, Deva Ramanan, and Mahadev Satyanarayanan. Mega-nerf: Scalable construction of large-scale nerfs for virtual fly-throughs. In *CVPR*, pages 12922–12931, 2022. 1, 3, 6, 7
- [51] Haithem Turki, Vasu Agrawal, Samuel Rota Bulò, Lorenzo Porzi, Peter Kotschieder, Deva Ramanan, Michael Zollhöfer, and Christian Richardt. Hybridnerf: Efficient neural rendering via adaptive volumetric surfaces. In *CVPR*, pages 19647–19656, 2024. 3
- [52] Zipeng Wang and Dan Xu. Pygs: Large-scale scene representation with pyramidal 3d gaussian splatting. *arXiv preprint arXiv:2405.16829*, 2024. 3
- [53] Zhou Wang, Alan C Bovik, Hamid R Sheikh, and Eero P Simoncelli. Image quality assessment: from error visibility to structural similarity. *TIP*, 13(4):600–612, 2004. 5, 6

- [54] Dejia Xu, Yifan Jiang, Peihao Wang, Zhiwen Fan, Humphrey Shi, and Zhangyang Wang. Sinnerf: Training neural radiance fields on complex scenes from a single image. In *ECCV*, pages 736–753, 2022. [3](#)
- [55] Linning Xu, Yuanbo Xiangli, Sida Peng, Xingang Pan, Nanxuan Zhao, Christian Theobalt, Bo Dai, and Dahua Lin. Grid-guided neural radiance fields for large urban scenes. In *CVPR*, pages 8296–8306, 2023. [3](#)
- [56] Daniel Yang, John J. Leonard, and Yogesh Girdhar. Seasplat: Representing underwater scenes with 3d gaussian splatting and a physically grounded image formation model. *arxiv*, 2024. [1](#)
- [57] Zhenpei Yang, Yuning Chai, Dragomir Anguelov, Yin Zhou, Pei Sun, Dumitru Erhan, Sean Rafferty, and Henrik Kretzschmar. Surfelgan: Synthesizing realistic sensor data for autonomous driving. In *CVPR*, pages 11118–11127, 2020. [1](#)
- [58] Chubin Zhang, Hongliang Song, Yi Wei, Yu Chen, Jiwen Lu, and Yansong Tang. Geolrm: Geometry-aware large reconstruction model for high-quality 3d gaussian generation. *arXiv preprint arXiv:2406.15333*, 2024. [3](#)
- [59] Hanyue Zhang, Zhiliu Yang, Xinhe Zuo, Yuxin Tong, Ying Long, and Chen Liu. Garfield++: Reinforced gaussian radiance fields for large-scale 3d scene reconstruction. *arXiv preprint arXiv:2409.12774*, 2024. [3](#)
- [60] Richard Zhang, Phillip Isola, Alexei A Efros, Eli Shechtman, and Oliver Wang. The unreasonable effectiveness of deep features as a perceptual metric. In *CVPR*, pages 586–595, 2018. [6](#)
- [61] Yuqi Zhang, Guanying Chen, and Shuguang Cui. Efficient large-scale scene representation with a hybrid of high-resolution grid and plane features. *Pattern Recognition*, 158: 111001, 2025. [3](#)

Momentum-GS: Momentum Gaussian Self-Distillation for High-Quality Large Scene Reconstruction

Supplementary Material

6. Quantitative Evaluation

VRAM. We report the peak VRAM usage during inference across five large-scale scenes, as shown in Tab. 6. Despite achieving superior reconstruction quality, our method, Momentum-GS, requires less VRAM compared to the purely 3D-GS-based approach. The VRAM usage, measured in MB, highlights the efficiency of our method. Notably, as scene complexity increases (*e.g.*, in MatrixCity[25]), the advantages of our method become even more pronounced. All experiments were conducted on Nvidia RTX 3090 GPUs with 24 GB of memory. Furthermore, CityGaussian[31] exceeds the 24 GB VRAM limit in certain scenes, such as Building[50] and MatrixCity, resulting in out-of-memory errors.

| Scene | Building | Rubble | Residence | Sci-Art | MatrixCity |
|--------------------|-------------|-------------|-------------|-------------|-------------|
| CityGaussian [31] | 8977 | 5527 | 6494 | 2726 | 14677 |
| Momentum-GS (Ours) | 5830 | 4106 | 6419 | 6647 | 4616 |

Table 6. Peak VRAM usage (in MB) during inference.

Storage. We report the storage usage across five large-scale scenes, as shown in Tab. 7. Leveraging our hybrid representation, our method significantly reduces the number of parameters required for storage compared to purely 3D-GS-based methods. This reduction is especially notable in larger and more complex scenes, such as MatrixCity[25], where the storage savings are most substantial. Notably, as scene complexity increases (*e.g.*, in MatrixCity), the advantages of our method become even more pronounced, demonstrating its effectiveness in handling challenging scenarios. For clarity and consistency, storage usage is reported in GB.

| Scene | Building | Rubble | Residence | Sci-Art | MatrixCity |
|--------------------|----------------------|----------------------|----------------------|-------------|----------------------|
| CityGaussian [31] | 3.07 | 2.22 | 2.49 | 0.88 | 5.40 |
| Momentum-GS (Ours) | 2.45 (20.2%↓) | 1.50 (32.7%↓) | 2.00 (19.7%↓) | 0.97 | 2.08 (61.5%↓) |

Table 7. Storage usage (in GB).

Number of Voxels. We report the voxel count for each reconstruction model across four large-scale scenes, as shown in Tab. 8. Leveraging our hybrid representation, all Gaussians are dynamically predicted on-the-fly based on the

viewing positions, resulting in a variable number of Gaussians.

| Scene | Building | Rubble | Residence | Sci-Art | MatrixCity |
|--------|----------|--------|-----------|---------|------------|
| Voxels | 8.33M | 5.09M | 6.79M | 3.30M | 7.08M |

Table 8. Voxel counts for each scene.

Analysis of 6× Downsampling. In alignment with most previous methods [27, 31, 35, 50], we downsampled all images by a factor of 4, whereas DOGS [9] applied a higher downsampling rate of 6 or more. We observed that downsampling images by a factor of 6 produces significantly better results compared to a factor of 4, as the reconstruction difficulty decreases (*e.g.* high-frequency information is reduced) with higher downsampling rates. As shown in Tab. 9, our method achieves much better results when images are downsampled by a factor of 6.

7. More Visual Comparisons

We provide additional visual comparisons for the Building[50], Rubble[50], Residence[28], and Sci-Art[28] scenes. Our method consistently reconstructs finer details across these scenes. Notably, our approach demonstrates a superior ability to reconstruct luminance, as illustrated by the Sci-Art example shown in Fig. 6. While NeRF-based methods are capable of capturing luminance by leveraging neural networks to learn global features such as lighting, they tend to produce blurrier results compared to 3D-GS-based methods. This underscores the effectiveness of our hybrid representation, which combines the strengths of both NeRF-based and 3D-GS-based approaches.

| Scene | <i>Building</i> | | | <i>Rubble</i> | | | <i>Residence</i> | | | <i>Sci-Art</i> | | |
|---|-----------------|-----------------|--------------------|-----------------|-----------------|--------------------|------------------|-----------------|--------------------|-----------------|-----------------|--------------------|
| Metrics | PSNR \uparrow | SSIM \uparrow | LPIPS \downarrow | PSNR \uparrow | SSIM \uparrow | LPIPS \downarrow | PSNR \uparrow | SSIM \uparrow | LPIPS \downarrow | PSNR \uparrow | SSIM \uparrow | LPIPS \downarrow |
| DOGS [9] ($6\times\downarrow$) | 22.73 | 0.759 | 0.204 | 25.78 | 0.765 | 0.257 | 21.94 | 0.740 | 0.244 | 24.42 | 0.804 | 0.219 |
| Momentum-GS (Ours, $4\times\downarrow$) | <u>23.23</u> | <u>0.815</u> | <u>0.194</u> | <u>25.93</u> | <u>0.827</u> | <u>0.201</u> | <u>22.21</u> | <u>0.818</u> | <u>0.197</u> | 23.02 | <u>0.856</u> | <u>0.205</u> |
| Momentum-GS (Ours, $6\times\downarrow$) | 23.76 | 0.841 | 0.153 | 26.67 | 0.863 | 0.153 | 22.61 | 0.849 | 0.150 | <u>23.20</u> | 0.876 | 0.156 |

Table 9. We present metrics for PSNR \uparrow , SSIM \uparrow , and LPIPS \downarrow on test views. The **best** and second best scores are highlighted.

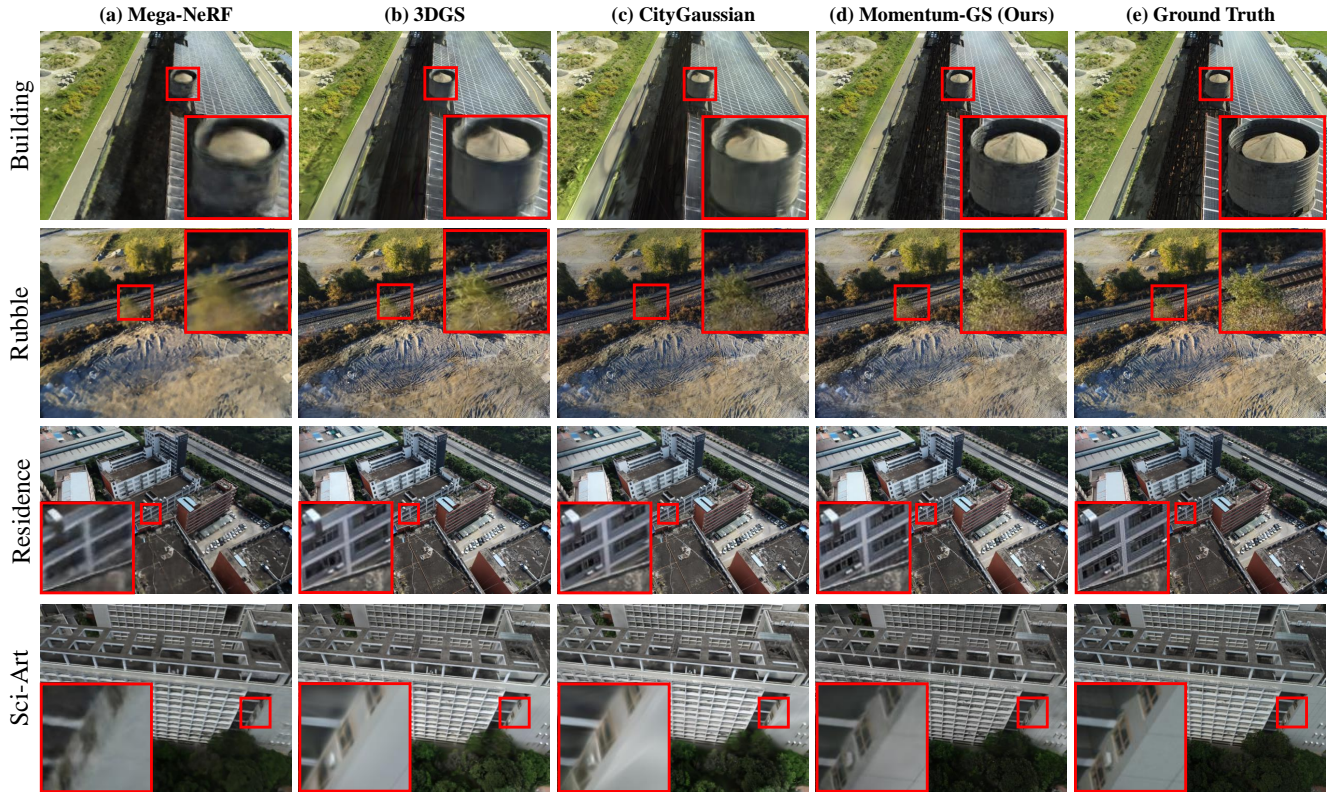


Figure 6. Qualitative comparisons of our Momentum-GS and prior methods across four large-scale scenes.